Journal of Alloys and Compounds 803 (2019) 826–833

Contents lists available at ScienceDirect

Journal of Alloys and Compounds

journal homepage: http://www.elsevier.com/locate/jalcom

Self-contained InGaN/GaN micro-crystal arrays as individually addressable multi-color emitting pixels on a deformable substrate

Dong Won Yang [a], Keundong Lee [b], Suhee Jang [a], Won Jun Chang [a], Su Han Kim [a], Jae Hyung Lee [a], Gyu-Chul Yi [b, **], Won Il Park [a, *]

[a] Division of Materials Science and Engineering, Hanyang University, 222, Wangsimni-ro, Seongdong-gu, Seoul, 04763, Republic of Korea
[b] Department of Physics and Astronomy, Institute of Applied Physics and Research Institute of Advanced Materials (RIAM), Seoul National University, 1, Gwanak-ro, Gwanak-gu, Seoul, 151-747, Republic of Korea

ARTICLE INFO

Article history:
Received 26 April 2019
Received in revised form
28 June 2019
Accepted 29 June 2019
Available online 29 June 2019

Keywords:
GaN
Micro-LED
Flexible LED
Multi-color emission
MOCVD

ABSTRACT

InGaN/GaN micro-crystals (μ-crystals) are self-contained and individually-addressable light emitting crystals that have unique potential in the development of ultra-small and ultra-high resolution pixels for next-generation displays. In this study, we explore the electrically-driven light emission behavior of vertically standing InGaN/GaN micro-crystals (μ-crystals) with well-defined crystal facets and tunable size. InGaN/GaN μ-crystals have hollow pedestals weakly bound to the substrate surface, thus enabling individual manipulation and/or collective transfer to other target surfaces. Cyclic bending tests and finite element analysis (FEA) of the strain distribution further highlight the excellent mechanical deformability of a device layout consisting of μ-crystal pixels embedded in a polymeric matrix. Light-emitting diodes (LEDs) with individual InGaN/GaN μ-crystals exhibit strong electroluminescence (EL) with unique features such as variations in emission spectra with respect to crystal diameter and driving voltage bias. Comparative analyses of photoluminescence, cathodoluminescence, and electric potential simulation indicate a strong correlation between the EL wavelengths and dominant emitting regions of InGaN/GaN polyhedral crystal planes. This is further supported by scanning transmission electron microscopy of quantum well structures, which strongly depend on both size and the crystal facets.

1. Introduction

The emergence of portable and wearable devices has led to an ever-increasing demand for next-generation displays that exhibit an ultra-high resolution, light weight, low power, and high efficiency, while simultaneously conforming to non-planar and/or variable surface geometries [1–5]. As an alternative to liquid crystal displays (LCDs), organic light-emitting diodes (OLEDs) have recently been used to create thinner, lighter, and flexible displays. However, OLEDs possess intrinsic limitations related to organic materials, such as low efficiency and poor stability, causing the 'burn-in' phenomenon [6,7]. In addition, the rapidly increasing cost and complexity of the fabrication processes (e.g., printing organic materials for red, green, and blue pixels and aligning shadow masks for metal electrodes), together with the lower brightness of OLEDs, poses great challenges for pixel size scale-down to the micro-scale [8].

Micro-LEDs (μ-LEDs) based on inorganic-semiconductors are being considered to overcome the limitations of existing display technologies [9–13]. The use of self-emissive μ-LEDs can simplify the display structure and decrease the overall device thickness by eliminating various components of conventional displays, such as color filters, backlight units, and thick encapsulation layers [14]. Driven by advances in GaN-based technology, extreme brightness and long-term operation can readily be achieved with existing GaN/InGaN multiple quantum well (QW) LEDs [15–17]. GaN/InGaN LEDs have a long life time (over 10 years) with reliable operation under a wide temperature range from −100 to 120 °C [14]. Moreover, a tunable band gap with varying In composition enables GaN/InGaN LEDs to cover the entire visible spectral range [11,18,19]. Nonetheless, conventional planar thin-film technology to implement multiple colors on a single chip substrate does not exist at this time. Alternatively, red, green, and blue pixels, independently fabricated from different substrates were transported to the target

* Corresponding author.
** Corresponding author.
E-mail addresses: gcyi@snu.ac.kr (G.-C. Yi), wipark@hanyang.ac.kr (W.I. Park).

https://doi.org/10.1016/j.jallcom.2019.06.374
0925-8388/

substrate through multiple transfer steps of (pick-up and drop-off) [20–22]. In addition to these complicated and expensive processes, smaller LED fragments are more susceptible to emission quenching through surface non-radiative recombination sites, further restricting the benefits of inorganic LEDs for ultra-small pixels [23–25].

In this regard, bottom-up-based epitaxial growth of one-dimensional (1D) InGaN/GaN crystals provides a unique alternative. Representative examples of this approach were implemented by growing InGaN/GaN QWs on nanoscale templates (e.g., GaN nanorods and nanocones, and ZnO nanotubes and nanowalls). QWs on these 1D crystals have several advantages over conventional QWs on planar bulk crystals, such as a reduced quantum-confined Stark effect, higher light extraction efficiency, and lower dislocation density [26,27]. In addition, multi-color emission on the same substrate can be realized via In composition and/or width variation in InGaN QWs, depending on their nanoscale diameter [12,13,26]. The shadowing effect and interplay between impingement and surface diffusion of adatoms have been suggested as key mechanisms; however, these phenomena have mostly been examined at the nanoscale level [12,28]. Despite the potential of these structures as light sources, it remains unclear whether such strategies can be expanded to a more perceptually meaningful scale so that they are compatible with pixel sizes (e.g., several to several tens of micrometers). Moreover, InGaN/GaN crystal arrays grown directly on rigid substrates would require additional high-cost processes for separation and transfer in practical display applications [20–22,29].

Herein, we explore the potential of InGaN/GaN-based microcrystals (μ-crystals) as individually-addressable, self-contained, and color-tunable emitting pixels for LEDs that are amenable to integration on flexible substrates. Based on optical and structural analyses of InGaN/GaN QWs simultaneously grown on polyhedral μ-crystals, we ensure strong size- and voltage-dependent multi-color emission behaviors considering crystal facets and size. Our study proposes design considerations for simultaneous growth and integration of multi-color pixel LEDs on a deformable substrate that can be applied to flexible or rollable displays, as well as user-friendly optoelectronics [30–33].

2. Experimental

2.1. GaN based μ-crystal arrays

Hexagonal-rod shaped ZnO micro-crystal arrays with variable diameters were epitaxially grown on a ZnO seed layer using a hydrothermal method, to be used as a sacrificial template for 3D InGaN/GaN crystal growth. The diameter and position of the ZnO hexagonal-rod array was controlled by using lithographically-patterned few-layer graphene sheets as a growth mask, in which the diameters of the holes were varied in the range of 3–14 μm. The detailed procedures were published elsewhere. The samples with a ZnO hexagonal-rod array were then deposited with undoped GaN (0.4 μm) by a home-built MOCVD (Metal organic chemical vapor deposition). To prevent the corrosion of ZnO crystals during the MOCVD process, initial GaN growth was performed at a relatively low temperature of 600 °C for 20 min, followed by high temperature growth at 1050 °C for 60 min. NH_3 and triethylgallium (TEGa) with an H_2 carrier gas at a bubbler temperature of 5 °C were used as precursors with typical flow rates of 400 and 30 sccm, respectively. The reactor pressure was held at 100 mbar. The samples were then transferred to a vertical-type MOCVD reactor to further deposit n-type GaN, GaN/InGaN MQWs, and p-type GaN, subsequently. For n-type and p-type doping, ditertiary butyl silane (DTBSi) and bis(-cyclopentadienyl)magnesium (Cp2Mg) were introduced for Si and Mg doping sources, respectively, while NH_3 and trimethylgallium (TMGa) were used as precursors. During the InGaN/GaN MQW layer growth, trimethylindium (TMI) was introduced as the Indium precursor.

2.2. InGaN/GaN μ-LEDs

GaN μ-LED arrays were fabricated using bottom graphene and top Ni/Au layers as the bottom n-type and top p-GaN contact electrodes, respectively. After growing GaN n-type and p-type layers on the ZnO crystals (grown in the holes in the graphene electrodes), the gaps between the GaN crystals were filled with polyimide polymer (PI) by spin-casting, to prevent current leakage between the top and bottom electrodes. Following spin-casting of the PI, the samples were etched with O_2 plasma until only the upper parts of the GaN crystals were exposed. A top electrode was fabricated on the p-GaN surface by deposition of metal films (composed of a 20-nm Ni layer and a 25-nm Au layer) over a photolithographically patterned photoresist (AZ5214) layer, followed by lift-off. The sample was then annealed at 300 °C to form an ohmic contact. A bottom electric contact to the n-GaN layers was made through the underlying MLG layer, on one side of which an Ag paste was applied for electric probing. To transfer InGaN/GaN μ-LEDs from the flexible substrate, the InGaN/GaN μ-LED arrays embedded with the PI layers were detached from the Sapphire/GaN substrates by etching away the ZnO seed layer located between the graphene layers and GaN substrate in an HF:H_2O (1:10) diluted solution. A bottom electrode (composed of a 20-nm Ti layer and a 25-nm Al layer) was then deposited on the bottom of the n-GaN surface, after fixing the μ-LEDs embedded with PI to Cu foil using an Ag adhesive.

2.3. FEA modeling

FEA (Finite element analysis) simulations were performed to visualize the strain and electric potential distribution for the InGaN/GaN μ-crystals. For FEA simulation of the strain distribution, we used the following parameters: GaN (Young's modulus: 1.81×10^{11} Pa, Poisson's ratio: 0.352, c-axis Wurtzite crystal with a 1.5-μm wall thickness and 3-μm void), polyimide (Young's modulus: 3.1×10^{9} Pa, Poisson's ratio: 0.34, thickness: 5 μm), and Cu (thickness: 25 μm). For FEA simulation of the electric potential distribution, the following parameters were used for n-GaN and p-GaN materials: n-GaN (Band gap: 3.39 eV, Doping concentration: n-type, ND: $3 \times 10^{18}/cm^3$, thickness: 1.5–2 μm) and p-GaN (Band gap: 3.39 eV, Doping concentration: p-type, NA: $1 \times 10^{18}/cm^3$, thickness: 0.1–0.2 μm). The metal contacts on the crystals were set as ideal ohmic contacts on both the p- and the n-GaN. The bottom contact was held at 0 Vs for all simulations.

3. Results and discussion

3.1. Fabrication of InGaN/GaN μ-crystal LEDs

Growth of the μ-crystals, consisting of p-type GaN, InGaN/GaN multiple QWs, and n-type GaN layers, and fabrication of the micro-pixel LED arrays are shown schematically in Fig. 1a and b, respectively. Our approach to simultaneous growth of different sized InGaN/GaN μ-crystals exploits a series of ZnO hexagonal rods (*h*-rods) possessing different diameters (i.e., hexagon diagonals), that were grown via a low-temperature hydrothermal method, and used as sacrificial templates [34]. The use of well-established ZnO crystal growth determines the position, size, and morphology of the resulting crystals [34–39]. The final stage InGaN/GaN crystals have polyhedral structures, consisting of the upper part of the truncated hexagonal prism tip and the lower part of the hexagonal

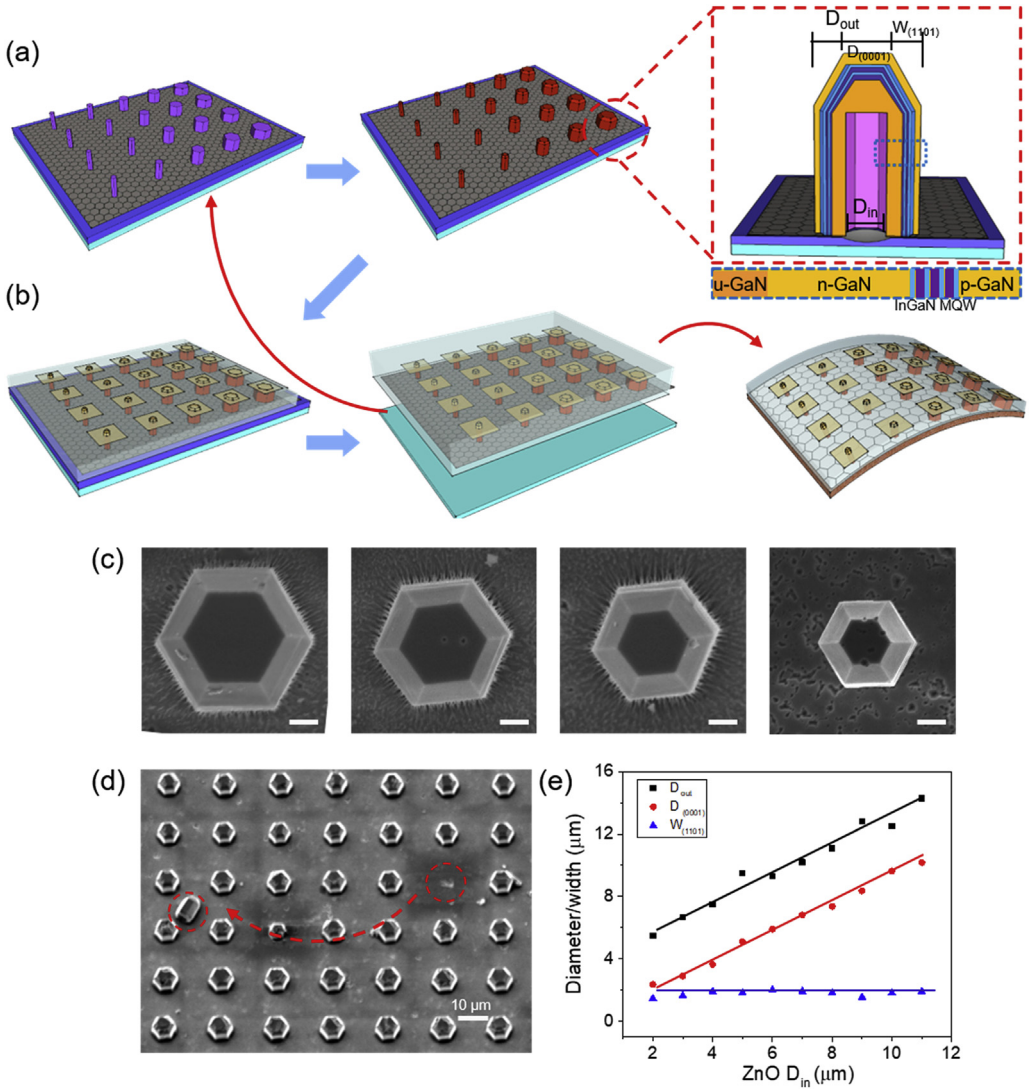

Fig. 1. a) Schematic illustration of the heteroepitaxial growth of InGaN/GaN μ-crystals on the size and position controlled ZnO rod template. The inset schematically shows the cross-sectional structure of the μ-crystal and definitions of the parameters used in this study. b) Schematics illustrating LED device fabrication on a rigid substrate (left panel) and on a flexible Cu foil (right panel). c) SEM images of InGaN/GaN LED μ-crystals with decreasing diameters from 11 μm to 5 μm. Scale bars: 2 μm. d) Top view of an InGaN/GaN μ-crystal array. e) Plots of D_{out}, $D_{(0001)}$, and $W_{(1101)}$ versus D_{in} for the InGaN/GaN μ-crystals.

walls (Fig. 1a, right panel). In this work, we employed a series of ZnO *h*-rods with diameters of ~2, 4, 6, and 8 μm. The outer diameters D_{out} (lengths) of the InGaN/GaN crystals were measured to be ~5 (17), 7 (16), 9 (15), and 11 (14) μm for ZnO *h*-rods with the diameters (lengths) of ~2, 4, 6, 8 μm, respectively (Fig. 1c, e). Given that the inner diameters D_{in} of the InGaN/GaN crystals are identical to the diameters of the ZnO *h*-rods, the thickness of the lower part of the hexagonal wall is ~1.5 μm, regardless of D_{out} and D_{in}. It is also important to note that the diameter of the top hexa-planes (i.e., (0001) planes) increase linearly with D_{out}, whereas the width of the side planes of the truncated hexagonal prism (i.e., $(1\bar{1}01)$ planes) is kept constant at 2 μm (Fig. 1e, blue dots).

The ZnO *h*-rod is gradually etched from the side of the crystals during the metal-organic chemical vapor deposition (MOCVD) growth of the GaN and InGaN/GaN QW layers, whereas the ZnO seed layer, protected by multilayer graphene (MLG) sheets, remains nearly stable. This MOCVD process leads to the formation of vertically standing hollow crystals on the substrate surface. This feature is particularly advantageous for increasing light extraction efficiency since the existence of a hollow air void at the core of the μ-crystals can suppress the total internal reflection [40,41]. Moreover, individual InGaN/GaN μ-crystals are weakly anchored to the underlying substrate by van der Waals interactions between the side wall bottoms and the MLG surface. The μ-crystals can be easily detached (i.e., plugged-out) from the substrates with no etching-driven surface damage (see Fig. 1d, in which one InGaN/GaN μ-crystal is detached from the substrate using mechanical stress and laying on around).

Fig. 1b schematically shows the fabrication process of μ-LEDs with InGaN/GaN μ-crystals on rigid and soft substrates (left and right panels, respectively). To fabricate top electrodes on the vertically-standing crystals, the gaps between the μ-crystals were filled with polyimide (PI) polymer using spin-casting, followed by oxygen plasma etching until only the upper parts (height of ~2 μm) of the crystals were exposed. Top electrodes (composed of a 20-nm Ni layer and a 25-nm Au layer) were then defined by photolithography, metal evaporation, and lift-off, while the bottom common electric contact was fabricated on the underlying MLG/substrate. To ensure ohmic contacts, thermal annealing was performed at 300 °C for 10 min. On the other hand, the layout of near-

free-standing InGaN/GaN μ-crystals embedded in polyimide (PI) over MLG offers advantages for damage-free transfer to non-planar and/or variable surface geometries. First, the whole LED array was easily separated from the growth substrate using selective etching of the ZnO interlayer in weak acid (HF:H_2O 1:10 diluted solution), where both the MLG and GaN crystals are chemically intact. Second, the self-contained InGaN/GaN μ-crystals exhibit enhanced mechanical flexibility so as to accommodate flexural (bending) deformation without fracture. To demonstrate the advantages of this type of structure, we tested the isolation (i.e., pick-up) of the thin layer of the LED array (after encapsulation with PI) and replacement (i.e., drop-off) onto the 25-μm-thick copper foil (see the Methods for a detailed description of the transfer procedure). The scanning electron microscopy (SEM) image of the substrate before and after the transfer show that most of the InGaN/GaN μ-crystals (over 90%) were well detached from the substrate (Fig. S1). The remaining sapphire/GaN substrate can also be reused after cleaning with O_2 plasma and aqua regia (Fig. S1).

3.2. Optoelectrical characteristics of InGaN/GaN μ-LEDs

Photographic images in Fig. 2a show the operation of the flexible InGaN/GaN LED, (consisting of 2×3 μ-crystals) on copper foil. Electroluminescent (EL) emission was quite strong and clearly visible by the naked eye regardless of whether the LED on the substrate was flat or bent with a radius of curvature of less than ~0.7 cm, corresponding to a tensile strain of ~0.038%. Current-voltage (I–V) characteristic curves of the device also exhibited

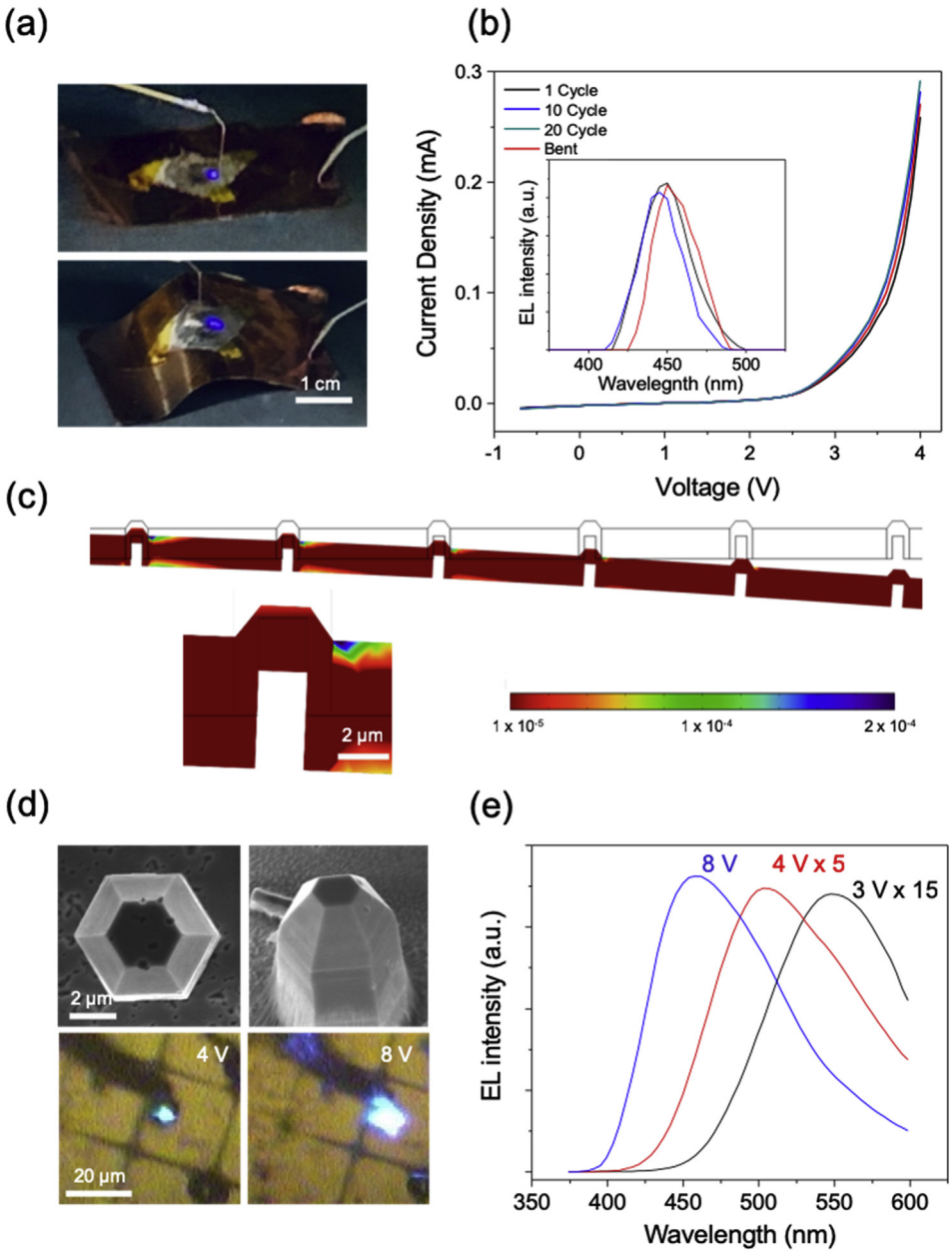

Fig. 2. a) Photographs of light emission from a flexible InGaN/GaN μ-crystal LED under the flat state and bent state (bending radius of 6.5 mm). b) I–V characteristic curves and EL spectra (inset) as a function of bending cycles. c) FEA simulation of the strain for the InGaN/GaN μ-crystal array embedded in PI (thickness ~5 μm) on 25-μm copper foil under a bending radius of 6.5 mm, showing only ~0.005% maximum strain applied in each crystal. d) SEM images (tops) and microscopy images of the light emission from the 5-μm crystal. e) Normalized EL spectra, under different bias voltages.

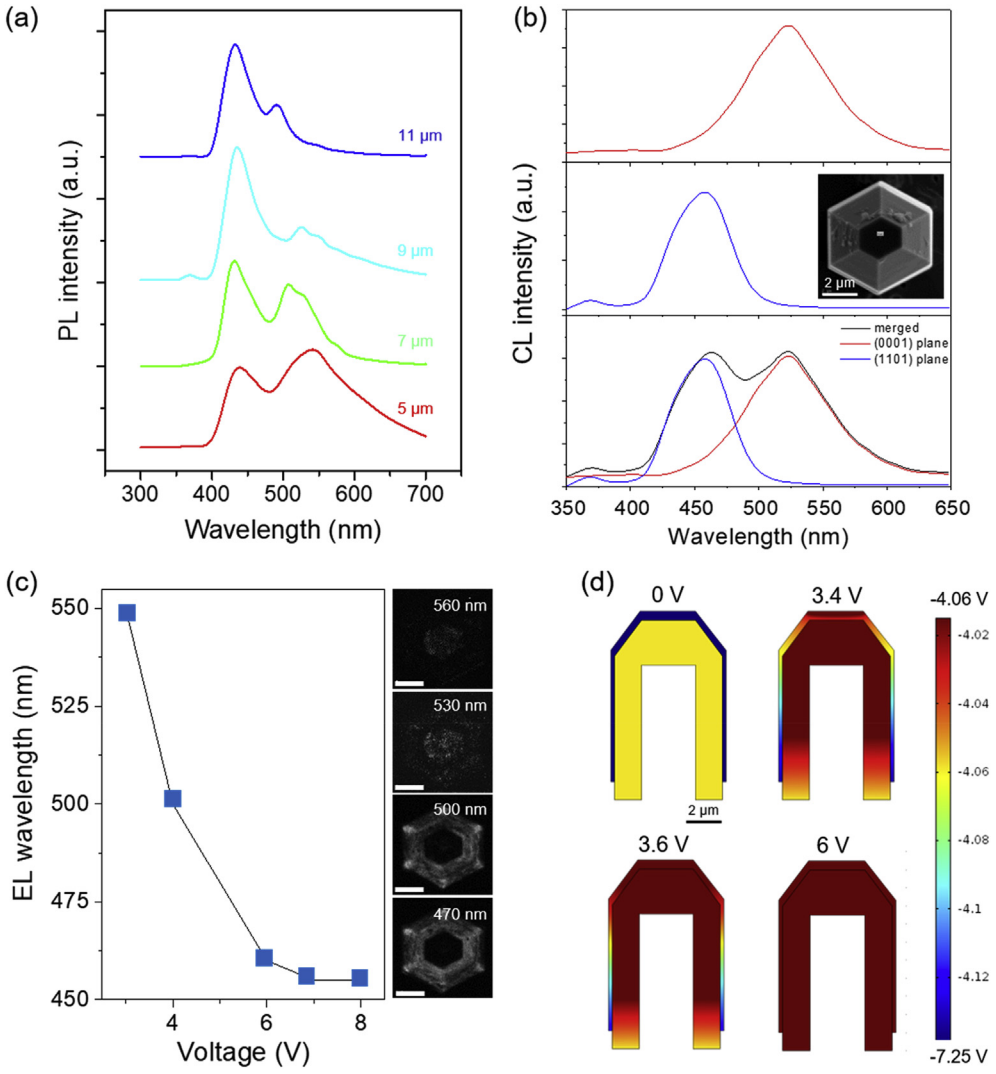

Fig. 3. a) Normalized PL spectra of InGaN/GaN μ-crystals with different diameters. b) CL spectra of the InGaN/GaN MQWs depending on measurement sites: top (0001) plane (top panel), (1$\bar{1}$01) plane (middle panel), and merged (bottom panel). Inset: top-view SEM image of the μ-crystal with measurement sites marked by crosses. c) Variations of EL emission wavelength of a 5-μm-diameter InGaN/GaN crystal LED depending on bias voltage (right), juxtaposed with CL mapping images at corresponding wavelengths. Scale bars: 2 μm. d) FEA simulation results of electric potential distributions for a GaN-based p-n junction crystal depending on the bias voltage.

typical rectifying transport behavior, without noticeable change in the flat state versus those in the bent state. A comparison of the μ-LED after dozens of bending cycles shows a negligible change in the I–V curves (less than 5% in voltage for 0.26 mA) (Fig. 2b). Meanwhile, there is a slight change in the EL spectra of the μ-LED (inset in Fig. 2b). We believe this is due to the measuring error rather than physical change of the device, given that EL spectra are very sensitive to optical alignment. Fig. 2c shows the finite element analysis (FEA) simulation results of the strain distribution of the GaN μ-crystals embedded in PI on the Cu substrate (5-μm thickness) that is mechanically bent with a radius of curvature identical to the experimental condition. The FEA simulation shows that the maximum strain applied in the μ-crystals is less than 0.005%, which is significantly lower than that in the soft matrix of PI, 0.02%, demonstrating the advantage of our device layout with excellent mechanical deformability. The mechanical characteristics can be further improved by placing the active layers near the neutral mechanical plane.

Importantly, we observed a change in emission wavelength with respect to the applied bias voltages that can be attributed to variation in luminescent characteristics from the polyhedral crystal planes. This characteristic can be advantageous as it allows multi-color emission capabilities from single devices. However, at the same time it can be disadvantageous because it limits the ability to control the brightness of the LED pixel. In order to further investigate this behavior, we fabricated the μ-LED array by defining independently addressable electrodes on top of each crystal (Fig. 2d). EL spectra from the single μ-crystal with D_{out} (that is, hexagon diagonal) of 5 μm is shown in Fig. 2e, which demonstrates the large change in the emission wavelength from 550 nm to 440 nm as the bias voltage increased from 3 V to 8 V. In addition, a careful comparison of EL emissions at the different bias voltages shows not only change in the emission color, but also a widening of the emitting area, from the top planes at a lower bias (4 V) and to the side planes (8 V) (see optical images in Fig. 2e). Similar behaviors can be found in μ-LEDs with different sized crystals, despite the fact that larger crystals exhibit an overall blue shift of EL emissions under an identical bias. For example, the μ-LED with an 11-μm diameter crystal shows an emission shift from 530 to 420 nm with the bias voltage from 3 V to 8 V (Fig. S2).

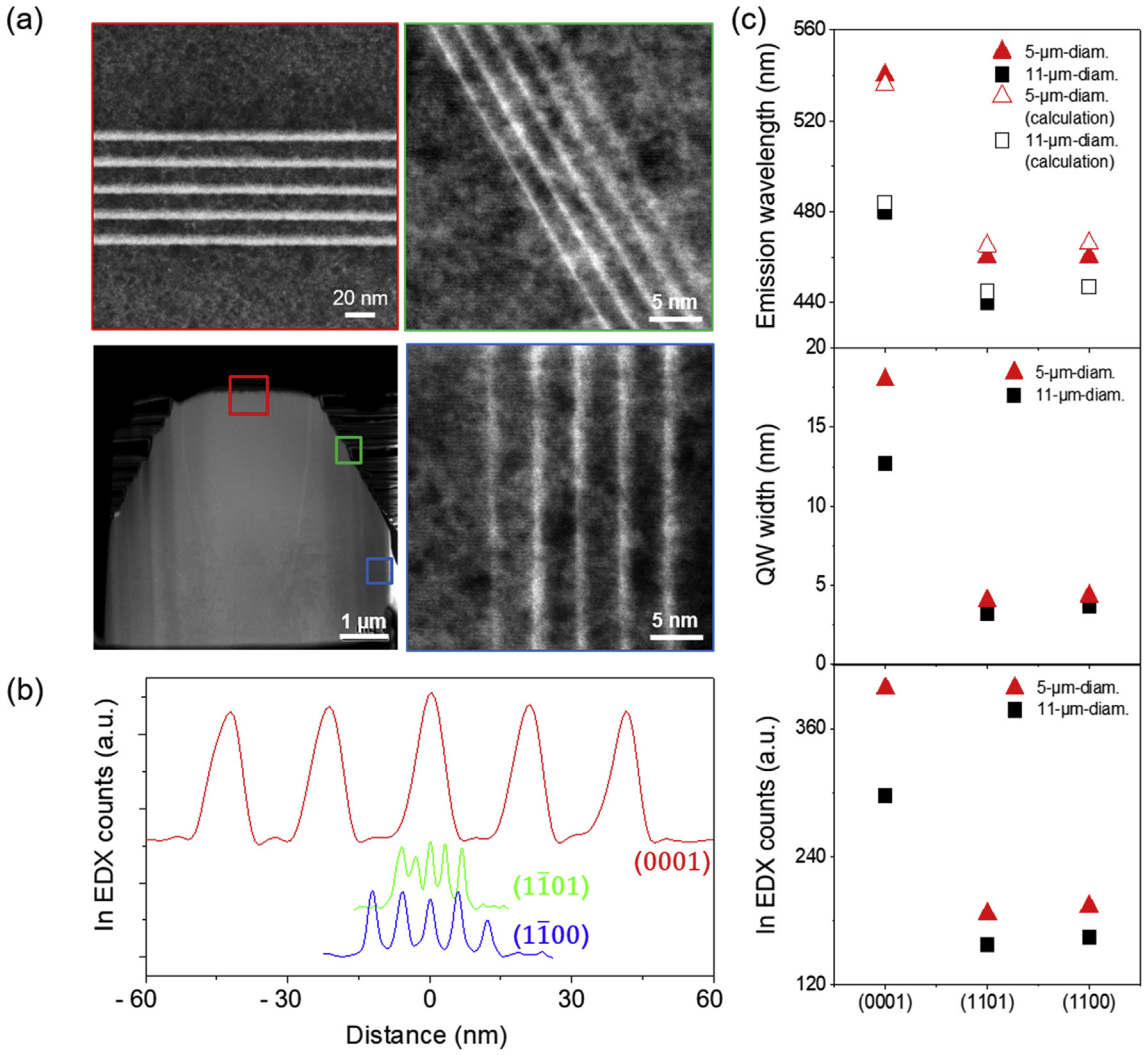

Fig. 4. a) A STEM image for cross-sectional InGaN/GaN μ-crystals with D_{out} of 5 μm, taken at the (0001), (1$\bar{1}$01), and (1$\bar{1}$00) planes, marked by red, green and blue squares, respectively. b) In EDX counts profiles derived from STEM-EDX analysis along the (0001), (1$\bar{1}$01), and (1$\bar{1}$00) planes in the 5-μm crystal, showing higher In-content and increased width of InGaN well layers in the (0001) plane. c) Plots of In EDX counts, QW width, and emission wavelength versus crystal planes for the μ-crystals with a D_{out} of 5 μm (red triangle) and 11 μm (black square). The simulation results for the expected emission wavelengths were plotted in open triangles and squares. (For interpretation of the references to color in this figure legend, the reader is referred to the Web version of this article.)

3.3. PL and CL analysis of multi-color emission characteristics

To elucidate the underlying mechanism of diameter and bias-dependent EL characteristics, we performed in-depth photoluminescence (PL) and cathodoluminescence (CL) measurements on the InGaN/GaN μ-crystals. Fig. 3a shows a series of PL spectra collected from individual crystals with increasing D_{out}, from 5 μm to 11 μm. Interestingly, all PL spectra exhibit two domains of the blue wavelength regime (~400–500 nm) and the green-yellow wavelength (~500–650 nm) regime. The PL spectra in the blue regime is characterized by a common single Gaussian peak centered at 440 nm, regardless of the D_{out}, whereas those in the green-yellow regime have broader emission bands consisting of several emission peaks. In addition, the green-yellow emission bands show markedly different features with respect to crystal size; as D_{out} decreases, an overall increase in the relative intensity, broadening and red-shift of the emission bands gradually occur. We observed analogous two-emission peaks from the CL spectra, and further confirmed that the peaks are position-specific, through excitation using a position-fixed e-beam. A representative example is shown in Fig. 3b, while only a green emission peak was dominantly observed at the top (0001) plane of the crystal with D_{out} of 5 μm, a blue emission peak appears in the CL spectra measured at the side facets of the truncated hexagonal prism tip, corresponding to the (1$\bar{1}$01) plane. The CL spectra obtained from the crystal laying on the substrate surface also shows that the (1$\bar{1}$00) plane, the surface of the lower part of the hexagonal walls, also exhibits blue emission, similar to the (1$\bar{1}$01) plane (Fig. S3). By merging the two CL emission spectra, we obtain a spectrum that is quite similar to the PL spectrum measured at the same crystal diameter (Fig. 3b, bottom panel). Similar trends were also found in crystals of other sizes (Fig. S4).

Spatially resolved CL mapping images at different wavelengths further support the microscopic correlation between crystal facets and dominant emission peaks (right panels in Fig. 3c and Fig. S4c). Importantly, the plot showing the comparison of EL peak positions and CL mapping demonstrates that the change in emission wavelength, depending on applied bias voltage, is associated with a shift of the dominant EL emitting facets in the InGaN/GaN crystals (Fig. 3c). Given that p-GaN has relatively high resistance, several

hundred times higher than that of n-GaN, effective travel of hole carriers is very limited in the outer p-GaN shell regions, in contrast to the case of electrons in the inner n-GaN [12]. In this situation, the dominant regions of hole and electron recombination events would be determined primarily by hole injection, which is very sensitive to applied bias voltages. To visualize this effect, we performed FEA modeling of bias voltage-dependent electric-potential distributions for a 5-μm-diameter crystal. As shown in Fig. 3d, applied bias concentrates predominantly on the p-n junction region of the top (0001) plane under a smaller voltage, but becomes equivalent across all p-n junction planes. As a result, electrically-driven hole-electron recombination events occur predominantly in the top region of the crystals at a lower bias, whereas the recombination sites broaden gradually to the $(1\bar{1}01)$ and $(1\bar{1}00)$ planes as the bias voltage increases (Fig. S5a).

3.4. STEM analysis of the cross-sectioned InGaN/GaN μ-crystals

To further support the mechanism of multi-color emissions as well as to correlate the emission wavelengths with multiple QW structures, we performed scanning transmission electron microscopy (STEM) analysis. Fig. 4a show STEM images of the cross-sectioned InGaN/GaN crystals with a D_{out} of 5 μm. From the In EDX counts versus distance measurements (Fig. 4b), we estimated In composition and thickness of the InGaN QW layers depending on microscopic crystal planes and diameters, as plotted in Fig. 4c. Comparative analysis of the results illustrates the following key features. First, there is little difference in In composition and the thickness of the InGaN QW layers between the side $(1\bar{1}01)$ and $(1\bar{1}00)$ planes, while both the In content and thickness increased greatly in the top (0001) plane. Second, the In content and thickness of InGaN QW layers in the (0001) planes also depend on the crystal diameter, as all increased by more than 30% in the 5-μm-diameter crystal, as compared to the 11-μm-diameter crystal (see also Fig. S6). On the basis of STEM analysis, we further calculated the emission wavelength for the corresponding finite square-well potential structures (top panel of Fig. 4c, open triangles and squares). Comparison of the results between theoretical predictions and experiments illustrates that the multi-color emissions observed in the InGaN/GaN crystals are strongly correlated with the variation of In compositions and the thickness over μ-crystal surfaces. The relative area ratio of the (0001) plane increases with increasing diameter (Fig. S5b), which plays another role in the diameter dependent luminescence characteristics.

Previous studies on QW structures in nanowires/rods showed a change in the composition and width with respect to diameter and interspacing of the nanocrystals [12,13,28]. The large difference in the diffusion lengths between Ga adatoms and In adatoms (1 μm versus 0.1 μm at high growth temperature) determines the effect area for the incorporation of each adatom to the tips of nanocrystals [13,28]. Considering the nanoscale (or sub-microscale) diffusion length of In adatoms, it has been shown that nanoscale diameter plays an important role in determining QW formation. Our observation, however, indicates that diffusion lengths of the In adatom on well-defined crystal facets become much longer, so as to influence QW formation on the microscale polyhedral facets. Of note, each facet has a different surface polarity, where surface migrations of adatoms on the non-polar $(1\bar{1}00)$ and semi-polar $(1\bar{1}01)$ planes are much faster than those on the polar (0001) plane [42–44]. In this circumstance, migration and settlement of the In adatoms, from surrounding lateral surfaces to the top plane, become sensitive to crystal size, resulting in an increase in In composition and thickness of the InGaN on the top (0001) polar surfaces, especially in smaller crystals. It is also noted that the size reduction was limited by the lithography step and the In concentration was fixed in this study, which thereby indicated that further improvement is desirable for diversifying the emission wavelength to cover the entire visible spectral range.

4. Conclusions

We demonstrated electrically-driven, multi-color emission from individually-addressable InGaN/GaN μ-crystal LEDs that are amenable to integration on flexible substrates. We performed in-depth optical and structural measurements and correlated bias-voltage and diameter-dependent wavelength change with variation in composition and thickness of multiple QWs on the polyhedral facets. Our study reveals the multicolor emission mechanism of self-contained InGaN/GaN QW μ-crystal LEDs, and further provides important design and growth considerations for realizing multi-color displays with ultra-small pixels on non-planar and/or non-rigid surfaces.

Acknowledgment

This work was supported by the National Research Foundation of Korea funded by the Ministry of Science, ICT and Future Planning of Korea (Nos. 2018R1A2B2006410, 2016K1A4A3914691) and the AFOSR/AOARD, USA (FA2386-18-1-4110). G.-C.Yi acknowledges this work supported by the National Research Foundation of Korea funded by the Ministry of Science, ICT and Future Planning of Korea (2015K1A1A2033332).

Appendix A. Supplementary data

Supplementary data to this article can be found online at https://doi.org/10.1016/j.jallcom.2019.06.374.

References

[1] M.K. Choi, J. Yang, K. Kang, D.C. Kim, C. Choi, C. Park, S.J. Kim, S.I. Chae, T.H. Kim, J.H. Kim, T. Hyeon, D.H. Kim, Wearable red-green-blue quantum dot light-emitting diode array using high-resolution intaglio transfer printing, Nat. Commun. 6 (2015) 7149.
[2] K. Chung, C.H. Lee, G.C. Yi, Transferable GaN layers grown on ZnO-coated graphene layers for optoelectronic devices, Science 330 (2010) 655–657.
[3] S. Kim, H.J. Kwon, S. Lee, H. Shim, Y. Chun, W. Choi, J. Kwack, D. Han, M. Song, S. Kim, S. Mohammadi, I. Kee, S.Y. Lee, Low-power flexible organic light-emitting diode display device, Adv. Mater. 23 (2011) 3511–3516.
[4] E.F. Schubert, J.K. Kim, Solid-state light sources getting smart, Science 308 (2005) 1274–1278.
[5] K.B. Lin, J. Xing, L.N. Quan, F.P.G. de Arquer, X.W. Gong, J.X. Lu, L.Q. Xie, W.J. Zhao, D. Zhang, C.Z. Yan, W.Q. Li, X.Y. Liu, Y. Lu, J. Kirman, E.H. Sargent, Q.H. Xiong, Z.H. Wei, Perovskite light-emitting diodes with external quantum efficiency exceeding 20 percent, Nature 562 (2018) 245–248.
[6] V.V. Jarikov, D.Y. Kondakov, Studies of the degradation mechanism of organic light-emitting diodes based on tris(8-quinolinolate)aluminum Alq and 2-tert-butyl-9,10-di(2-naphthyl)anthracene TBADN, J. Appl. Phys. 105 (2009), 034905.
[7] J.R. Sheats, H. Antoniadis, M. Hueschen, W. Leonard, J. Miller, R. Moon, D. Roitman, A. Stocking, Organic electroluminescent devices, Science 273 (1996) 884–888.
[8] C.D. Dimitrakopoulos, P.R.L. Malenfant, Organic thin film transistors for large area electronics, Adv. Mater. 14 (2002) 99–117.
[9] Y. Kim, S.S. Cruz, K. Lee, B.O. Alawode, C. Choi, Y. Song, J.M. Johnson, C. Heidelberger, W. Kong, S. Choi, K. Qiao, I. Almansouri, E.A. Fitzgerald, J. Kong, A.M. Kolpak, J. Hwang, J. Kim, Remote epitaxy through graphene enables two-dimensional material-based layer transfer, Nature 544 (2017) 340–343.
[10] J. Yoo, T. Ahmed, W. Tang, Y.J. Kim, Y.J. Hong, C.H. Lee, G.C. Yi, Single crystalline ZnO radial homojunction light-emitting diodes fabricated by metal-organic chemical vapour deposition, Nanotechnology 28 (2017), 394001.
[11] S. Pimputkar, J.S. Speck, S.P. DenBaars, S. Nakamura, Prospects for LED lighting, Nat. Photon. 3 (2009) 179–181.
[12] J.H. Kim, B.U. Ye, J. Park, C.J. Yoo, B.J. Kim, H.Y. Jeong, J.H. Hur, J.K. Kim, J.L. Lee, J.M. Baik, Visible color tunable emission in three-dimensional light emitting diodes by MgO passivation of pyramid tip, Acs Appl. Mater. Inter. 7 (2015) 27743–27748.
[13] Y.H. Ra, R.J. Wang, S.Y. Woo, M. Djavid, S.M. Sadaf, J. Lee, G.A. Botton, Z.T. Mi,

Full-color single nanowire pixels for projection displays, Nano Lett. 16 (2016) 4608–4615.
[14] H.E. Lee, J.H. Shin, J.H. Park, S.K. Hong, S.H. Park, S.H. Lee, J.H. Lee, I.-S. Kang, K.J. Lee, Micro light-emitting diodes for display and flexible biomedical applications, Adv. Funct. Mater. 29 (2019), 1808075.
[15] X.L. Hu, F.A. Xiao, Q.B. Zhou, Y.D. Zheng, W.J. Liu, High-luminous efficacy green light-emitting diodes with InGaN/GaN quasi-superlattice interlayer and Al-doped indium tin oxide film, J. Alloy. Comp. 794 (2019) 137–143.
[16] J.T. Oh, Y.T. Moon, J.H. Jang, J.H. Eum, Y.J. Sung, S.Y. Lee, J.O. Song, T.Y. Seong, High-performance GaN-based light emitting diodes grown on 8-inch Si substrate by using a combined low-temperature and high-temperature-grown AlN buffer layer, J. Alloy. Comp. 732 (2018) 630–636.
[17] X.W. Wang, F. Liang, D.G. Zhao, D.S. Jiang, Z.S. Liu, J.J. Zhu, J. Yang, W.J. Wang, Effect of dual-temperature-grown InGaN/GaN multiple quantum wells on luminescence characteristics, J. Alloy. Comp. 790 (2019) 197–202.
[18] B.O. Jung, S.Y. Bae, S.Y. Kim, S. Lee, J.Y. Lee, D.S. Lee, Y. Kato, Y. Honda, H. Amano, Highly ordered catalyst-free InGaN/GaN core-shell architecture arrays with expanded active area region, Nano Energy 11 (2015) 294–303.
[19] S. Nakamura, M. Senoh, N. Iwasa, S. Nagahama, High-power ingan single-quantum-well-structure blue and violet light-emitting-diodes, Appl. Phys. Lett. 67 (1995) 1868–1870.
[20] A. David, T. Fujii, B. Moran, S. Nakamura, S.P. DenBaars, C. Weisbuch, H. Benisty, Photonic crystal laser lift-off GaN light-emitting diodes, Appl. Phys. Lett. 88 (2006), 133514.
[21] T.I. Kim, Y.H. Jung, J.Z. Song, D. Kim, Y.H. Li, H.S. Kim, I.S. Song, J.J. Wierer, H.A. Pao, Y.G. Huang, J.A. Rogers, High-efficiency, microscale GaN light-emitting diodes and their thermal properties on unusual substrates, Small 8 (2012) 1643–1649.
[22] W.S. Wong, T. Sands, N.W. Cheung, M. Kneissl, D.P. Bour, P. Mei, L.T. Romano, N.M. Johnson, Fabrication of thin-film InGaN light-emitting diode membranes by laser lift-off, Appl. Phys. Lett. 75 (1999) 1360–1362.
[23] D. Hwang, A. Mughal, C.D. Pynn, S. Nakamura, S.P. DenBaars, Sustained high external quantum efficiency in ultrasmall blue III-nitride micro-LEDs, Appl. Phys. Express 10 (2017), 032101.
[24] F. Olivier, A. Daami, C. Licitra, F. Templier, Shockley-Read-Hall and Auger non-radiative recombination in GaN based LEDs: a size effect study, Appl. Phys. Lett. 111 (2017), 022104.
[25] P.F. Tian, J.J.D. McKendry, J. Herrnsdorf, S. Watson, R. Ferreira, I.M. Watson, E.D. Gu, A.E. Kelly, M.D. Dawson, Temperature-dependent efficiency droop of blue InGaN micro-light emitting diodes, Appl. Phys. Lett. 105 (2014), 171107.
[26] J.H. Kim, Y.H. Ko, J.H. Cho, S.H. Gong, S.M. Ko, Y.H. Cho, Toward highly radiative white light emitting nanostructures: a new approach to dislocation-eliminated GaN/InGaN core-shell nanostructures with a negligible polarization field, Nanoscale 6 (2014) 14213–14220.
[27] Y.C. Sim, S.H. Lim, Y.S. Yoo, M.H. Jang, S. Choi, H.S. Yeo, K.Y. Woo, S. Lee, H.G. Song, Y.H. Cho, Three-dimensional GaN dodecagonal ring structures for highly efficient phosphor-free warm white light-emitting diodes, Nanoscale 10 (2018) 4686–4695.
[28] H. Sekiguchi, K. Kishino, A. Kikuchi, Emission color control from blue to red with nanocolumn diameter of InGaN/GaN nanocolumn arrays grown on same substrate, Appl. Phys. Lett. 96 (2010), 231104.
[29] H.E. Lee, J.H. Choi, S.H. Lee, M.J. Jeong, J.H. Shin, D.J. Joe, D.H. Kim, C.W. Kim, J.H. Park, J.H. Lee, D.S. Kim, C.S. Shin, K.J. Lee, Monolithic flexible vertical GaN light-emitting diodes for a transparent wireless brain optical stimulator, Adv. Mater. 30 (2018), 1800649.
[30] C.M. Kang, S.J. Kang, S.H. Mun, S.Y. Choi, J.H. Min, S. Kim, J.P. Shim, D.S. Lee, Monolithic integration of AlGaInP-based red and InGaN-based green LEDs via adhesive bonding for multicolor emission, Sci. Rep. 7 (2017) 10333.
[31] J. Kim, P. Gutruf, A.M. Chiarelli, S.Y. Heo, K. Cho, Z.Q. Xie, A. Banks, S. Han, K.I. Jang, J.W. Lee, K.T. Lee, X. Feng, Y.G. Huang, M. Fabiani, G. Gratton, U. Paik, J.A. Rogers, Miniaturized battery-free wireless systems for wearable pulse oximetry, Adv. Funct. Mater. 27 (2017), 1604373.
[32] T.Z. Wu, C.W. Sher, Y. Lin, C.F. Lee, S.J. Liang, Y.J. Lu, S.W.H. Chen, W.J. Guo, H.C. Kuo, Z. Chen, Mini-led and micro-LED: promising candidates for the next generation display technology, Appl. Sci. 8 (2018) 1557.
[33] M. Zhang, M.Q. Wang, Z. Yang, J.J. Li, H.W. Qiu, Preparation of all-inorganic perovskite quantum dots-polymer composite for white LEDs application, J. Alloy. Comp. 748 (2018) 537–545.
[34] D.W. Yang, D. Yoo, W.W. Lee, J.M. Lee, G.C. Yi, W.I. Park, Three-dimensionally-architectured GaN light emitting crystals, CrystEngComm 19 (2017) 2007–2012.
[35] S.B. Kim, S. Kim, S.S. Kwon, W.W. Lee, J.S. Kim, W.I. Park, Large-scale synthesis of vertically aligned ZnO hexagonal nanotube-rod hybrids using a two-step growth method, J. Am. Ceram. Soc. 96 (2013) 3500–3503.
[36] J.M. Lee, Y.S. No, S. Kim, H.G. Park, W.I. Park, Strong interactive growth behaviours in solution-phase synthesis of three-dimensional metal oxide nanostructures, Nat. Commun. 6 (2015) 6325.
[37] W.W. Lee, S. Chang, D.W. Yang, J.M. Lee, H.G. Park, W.I. Park, Three-dimensional epitaxy of single crystalline semiconductors by polarity-selective multistage growth, CrystEngComm 18 (2016) 8262–8269.
[38] W.W. Lee, J. Yi, S.B. Kim, Y.H. Kim, H.G. Park, W.I. Park, Morphology-controlled three-dimensional nanoarchitectures produced by exploiting vertical and in-plane crystallographic orientations in hydrothermal ZnO crystals, Cryst. Growth Des. 11 (2011) 4927–4932.
[39] J.J. Cheng, S.M. Nicaise, K.K. Berggren, S. Gradecak, Dimensional tailoring of hydrothermally grown zinc oxide nanowire arrays, Nano Lett. 16 (2016) 753–759.
[40] Y.J. Moon, D. Moon, J. Jang, J.Y. Na, J.H. Song, M.K. Seo, S. Kim, D. Bae, E.H. Park, Y. Park, S.K. Kim, E. Yoon, Microstructured air cavities as high-index contrast substrates with strong diffraction for light-emitting diodes, Nano Lett. 16 (2016) 3301–3308.
[41] Y.S. Yoo, H.G. Song, M.H. Jang, S.W. Lee, Y.H. Cho, Electrically driven, highly efficient three-dimensional GaN-based light emitting diodes fabricated by self-aligned twofold epitaxial lateral overgrowth, Sci. Rep. 7 (2017) 9663.
[42] D. Min, D. Park, K. Lee, O. Nam, Colour-crafted phosphor-free white light emitters via in-situ nanostructure engineering, Sci. Rep. 7 (2017) 44148.
[43] K. Nishizuka, M. Funato, Y. Kawakami, Y. Narukawa, T. Mukai, Efficient rainbow color luminescence from InxGa1-xN single quantum wells fabricated on {11(2)over-bar2} microfacets, Appl. Phys. Lett. 87 (2005), 231901.
[44] A. Tanaka, R.J. Chen, K.L. Jungjohann, S.A. Dayeh, Strong geometrical effects in submillimeter selective area growth and light extraction of GaN light emitting diodes on sapphire, Sci. Rep. 5 (2015) 17314.